

Application of Three Types of Aminated Lignins for Efficient Removal of Cd(II) and Pb(II) Ions in Aqueous Solution

Ji Won Heo,^a Liangliang An,^a Jiansong Chen,^a Min Soo Kim,^a Sang-Deok Lee,^b and Yong Sik Kim^{a,*}

Lignin is a renewable natural aromatic polymer that is generated as a co-product during lignocellulosic biorefinery processes, and it has been applied widely as a functional biomaterial. In this study, the adsorption behavior of Cd(II) and Pb(II) metal ions was investigated *via* ion chelation using aminated lignins (ALs) with primary, secondary, and tertiary amine groups. ALs exhibited optimal Cd(II) and Pb(II) adsorption capacities in solution under neutral conditions due to their chelating, electrostatic, and cationic- π interactions with metal ions. The AL with the primary amine group showed the highest adsorption capacities for both Cd(II) and Pb(II), reaching 83.2 and 159.7 mg·g⁻¹, respectively, followed by the ALs with secondary and tertiary amine groups. The adsorption kinetics and isotherm analysis demonstrated that all adsorption behaviors followed the Langmuir isotherm and pseudo-second-order kinetics. Thermodynamic studies revealed that the adsorption processes of Cd(II) and Pb(II) using the ALs were spontaneous and endothermic. These results demonstrate that ALs are promising adsorbents for the removal of Cd(II) and Pb(II) metal ions.

DOI: 10.15376/biores.17.4.5958-5983

Keywords: Amino-silane; Aminated lignin; Metal ions; Adsorption mechanism; Adsorption isotherm

Contact information: a: Department of Paper Science & Engineering, College of Forest and Environmental Sciences, Kangwon National University, Chuncheon 24341, Republic of Korea; b: Division of Forest Science, College of Forest and Environmental Sciences, Kangwon National University, Chuncheon 24341, Republic of Korea; *Corresponding author: yongsikk@kangwon.ac.kr

INTRODUCTION

Heavy metal ions pose potential risks to human health and environment because of their toxic, non-biodegradable, and bioaccumulative nature (Boamah *et al.* 2015; Duan *et al.* 2018; Liu *et al.* 2018). Heavy metals released to the environment are detected in river, ground, and surface waters, where the sediments accumulate to form hazardous materials (Gocht *et al.* 2001; Gaur *et al.* 2005). Cd(II), one of the most common heavy metals, is metabolized slowly in the human body (Boparai *et al.* 2013; Bian *et al.* 2015). Therefore, it accumulates in organs, such as the kidneys, and has a long half-life (Bian *et al.* 2015; Genchi *et al.* 2020). Cadmium is released into the environment during the combustion of fossil fuels, mineralization, cement production, electroplating, and manufacturing of batteries and pigments (Li *et al.* 2003b; Bian *et al.* 2015). Pb(II) is a poisonous trace metal, which is hazardous to public health, particularly to humans, even at a low concentration (10 $\mu\text{g}\cdot\text{L}^{-1}$) in drinking water (Wang *et al.* 2020b; Zhou *et al.* 2021). Lead is a potent water pollutant that is widely distributed in environmental water bodies owing to its extensive

applications in various industries, including chemical manufacturing of paint, batteries, and cosmetics, as well as in coal mining, extractive metallurgy, nuclear power plants, and military usage (Sekar *et al.* 2004; Shahabuddin *et al.* 2018). Because of the hazardous nature of Cd(II) and Pb(II) ions, they must be removed from industrial wastewater before its release to the environment (Awaleh and Soubaneh 2014; Shahabuddin *et al.* 2018). Various techniques have been proposed to address water pollution, including adsorption, solvent extraction, ion exchange, membrane filtration, biological treatment, and chemical oxidation (Dutta *et al.* 2001; Kadirvelu *et al.* 2003; He *et al.* 2008; Li *et al.* 2020). Among these techniques, adsorption remains a priority for environmental scientists because it is economical, fast, and environmentally friendly (Li *et al.* 2003a; Stafiej and Pyrzyska 2007; Yu *et al.* 2021).

Natural materials from industry and agricultural operations have been used as prospective “green” adsorbents (Kyzas and Kostoglou 2014; Pyrzyska 2019). For example, lignin is the most abundant natural aromatic polymer and is composed of various phenyl propane units (C₆–C₃) (Zong *et al.* 2018). It is a sustainable, cost-effective, and biodegradable biopolymer (Santander *et al.* 2021). Lignin-based adsorbents can be used to treat different water pollutants, including organic dyes and heavy metal ions, because of their remarkable three-dimensional network with a cross-linked structure of macromolecules and various functional groups (Wang *et al.* 2019; Santander *et al.* 2021). Despite their potential, many unmodified lignins have insufficient ability to adsorb metal ions (Lora and Glasser 2002). To overcome this limitation, lignin surface modification introduces functional groups with high affinity for metal ion chelation, which increase the adsorption capacity of adsorbents. A previous study showed that amine-functionalized lignins can selectively adsorb harmful dyes, such as methylene blue and Congo red (Heo *et al.* 2022). Chen *et al.* (2021) have reported that amine groups were grafted onto the lignin by 2-chloroethylamine hydrochloride, which offers the lignin a higher capacity to capture silver ions. In addition, lignins can be functionalized with amine groups to significantly enhance heavy metal removal from wastewater (Zhang *et al.* 2019b; Zhou *et al.* 2021). The amine group is a suitable functional group for the development of adsorbents. Since the nitrogen atom has a free electron doublet that can react with the metal cation, the amine group may be responsible for the uptake of the metal cation by the chelation and electrostatic interaction (Wamba *et al.* 2018; Gdula *et al.* 2019). However, since the amine group is easily protonated in an acidic solution, electrostatic repulsion with the metal cation can act. Therefore, it can be expected to exhibit excellent metal cation uptake under non-acidic conditions (Guibal 2004).

In this study, the adsorption behavior of harmful Cd(II) and Pb(II) heavy metal ions was investigated using aminated lignins (ALs) with primary, secondary, and tertiary amine groups. In the heavy metal ion adsorption experiment, the effects of the adsorbent dosage, setting time, pH, initial concentration of metal ions, and temperature were examined. The relationship between adsorption capacity and adsorption mechanisms was investigated using adsorption isotherms, adsorption kinetics, and thermodynamic studies. Furthermore, the change in the chemical structure of the adsorbent after heavy metal ion adsorption was analyzed using X-ray photoelectron spectroscopy (XPS), Fourier-transform infrared (FT-IR) spectroscopy, and scanning electron microscopy coupled with energy-dispersive X-ray spectroscopy (SEM-EDS) to examine the adsorption mechanism in detail.

EXPERIMENTAL

Materials

Methanol lignin (ML) was isolated from kraft lignin (Moorim Pulp and Paper Co., Ltd., South Korea) (An *et al.* 2020; Heo *et al.* 2022). (3-Aminopropyl)trimethoxysilane (APTMS; 97%), (*N*-methylaminopropyl)trimethoxysilane (MAPTMS; 95%), (*N,N*-dimethyl-3-amino)propyltrimethoxysilane (DMAPTMS; 96%), cadmium nitrate tetrahydrate ($\text{Cd}(\text{NO}_3)_2 \cdot 4\text{H}_2\text{O}$; 99.997 %), and lead(II) nitrate ($\text{Pb}(\text{NO}_3)_2$; 99.999%) were purchased from Sigma-Aldrich (St. Louis, MO, USA). Anhydrous methanol (99.9%), anhydrous toluene (99.8%), pyridine (99.5%), acetic anhydride (98%), 0.1 N sodium hydroxide solution, and 0.1 N hydrochloric acid solution were procured from Daejung Chemicals and Metals Co., Ltd. (Seoul, South Korea). All purchased chemicals were used without further purification.

Synthesis of Adsorbents (ALs)

ALs were prepared using the method described previously (Fig. 1) (Heo *et al.* 2022). In summary, ML (2 g) was dispersed in 100 mL of anhydrous toluene under agitation (350 rpm for 30 min in a 250 mL round-bottom flask). Amino-silane (APTMS, DAPTMS, or DMAPTMS; 18 mmol) was added dropwise under N_2 atmosphere and heated at 70 °C for 24 h. After the reaction, the suspension was filtered and washed several times with toluene. The solid obtained was dried in a vacuum oven at 40 °C for 72 h. The ALs were named PAL ($-\text{NH}_2$), SAL ($-\text{NHCH}_3$), and TAL ($-\text{N}(\text{CH}_3)_2$).

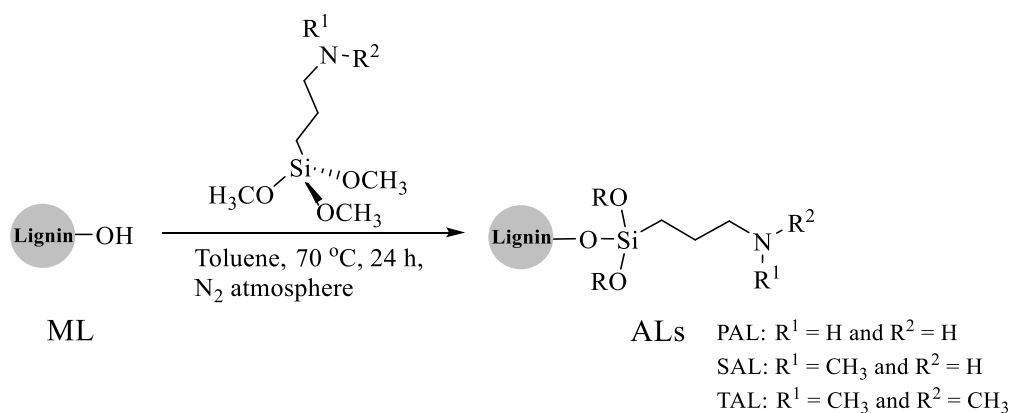


Fig. 1. Synthesis of three types of ALs

Adsorption Experiments

Heavy metal ion solutions with concentrations of 40 and 80 mg/L were prepared from $\text{Cd}(\text{NO}_3)_2$ and $\text{Pb}(\text{NO}_3)_2$, respectively. Next, 30 mL of the heavy metal ion solution was mixed with each AL (0.005 to 0.1 g) at different pH values (2 to 7) in an Erlenmeyer flask, and adsorption experiments were performed in a shaking incubator (IST-4075, JEIO TECH, Daejeon, South Korea) at a fixed speed (200 rpm) and different temperatures (298.15, 313.15 and 333.15 K) for 0 to 1440 min. The pH was adjusted using NaOH (0.1 N) and HCl (0.1 N) solutions. After the adsorption of heavy metal ions, the suspension was immediately filtered through a nylon membrane (NY020047A, HYUNDAI MICRO, Seoul, South Korea) with 0.20 μm pore size, and the concentrations of residual metal ions in the solution were determined using inductively coupled plasma optical emission spectroscopy (OPTIMA 7300 DV, PerkinElmer Korea, Seoul, South Korea). The emission

lines of Cd(II) and Pb(II) were 214.439 and 220.353 nm, respectively. For satisfactory precision, data with relative standard deviation (RSD) values less than 5% were used. The adsorption experiments were repeated at least 3 times, and the average values were used. The adsorbed amount (Q) and the adsorption efficiency (E) of Cd(II) and Pb(II) ions were calculated according to the following equations,

$$Q \text{ (mg/g)} = (C_0 - C_a) \times V/M, \quad (1)$$

$$E \text{ (\%)} = [(C_0 - C_a) / C_0] \times 100, \quad (2)$$

where C_0 and C_a are the initial and final concentrations, respectively, of the Cd(II) or Pb(II) solution, V is the volume (L) of the Cd(II) or Pb(II) solution, and M is the weight (g) of the adsorbent.

Characterization of Adsorbents Before and After Adsorption

The contents of different elements (C, N, and O) were determined using an elemental analyzer (FlashEA1112, Thermo Scientific, Wigan, UK) equipped with a thermal conductivity detector. The sizes of the ALs were analyzed *via* differential light scattering using a Malvern Mastersizer 3000 particle size analyzer (Malvern Instruments, Worcestershire, UK). The characterization of ALs was performed to elucidate the interactions of ALs with heavy metal ions. The chemical states of the elements on the surface of the lignin samples before and after the adsorption were analyzed using XPS (Thermo Scientific). The chemical structures of the ALs before and after adsorption were determined *via* FT-IR spectroscopy (Nicolet Summit, MA, USA) using the attenuated total reflectance tool. The spectra were recorded in the range of 500 to 4000 cm^{-1} at a resolution of 4.0 cm^{-1} with 128 scans. The morphologies and surface elemental contents of the lignin samples were determined using field-emission scanning electron microscopy (FE-SEM; JSM-7900F, JEOL, Tokyo, Japan) with an energy-dispersive X-ray spectrometer (EDS; JSM-7900F, JEOL).

RESULTS AND DISCUSSION

Characterization of ALs

FT-IR spectroscopy was employed to evaluate the chemical structure of ALs. As shown in Fig. S1, peaks in the spectra of the ALs confirmed the presence of amine groups and silicone-containing groups. These results were similar to those presented previously (Heo *et al.* 2022). In addition, acetylated ALs were used to evaluate the presence of amine groups. After the acetylation of the amine groups in PAL and SAL, a new peak appeared at 1645 cm^{-1} , which was assigned to the amide group (Fig. S1) (Chen *et al.* 2021). In the TAL spectrum, a peak at 1645 cm^{-1} was not observed, suggesting that the tertiary amine groups did not yield amide groups because the tertiary amine group did not react easily with acetic anhydride. This result confirmed that the chemical structures of the ALs contained three types of amine groups. In addition, elemental contents of the ALs were detected using elemental analysis, and the results are listed in Table S1. The N contents were in the following order: PAL (2.40%) > SAL (1.98%) > TAL (1.60%). Moreover, the N/C (%) of PAL was higher than those of the other ALs, suggesting that APTMS has higher reactivity toward hydroxyl groups and endows more amine groups into lignins. In this study, three types of aminated lignins were successfully synthesized.

The particle size of the adsorbent is a decisive parameter determining the efficiency of the adsorption process, and the particle sizes of the ALs are summarized in Table S1. The particle sizes of PAL (12.5 μm), SAL (12.0 μm), and TAL (9.3 μm) were higher than that of ML (8.7 μm). According to the previous study, the specific surface areas of the ALs were also higher than that of ML (5.2 $\text{m}^2\cdot\text{g}^{-1}$) and were in the following order: TAL (14.7 $\text{m}^2\cdot\text{g}^{-1}$) > SAL (11.2 $\text{m}^2\cdot\text{g}^{-1}$) > PAL (9.4 $\text{m}^2\cdot\text{g}^{-1}$) (Heo *et al.* 2022). The particle sizes and the specific surface areas of ALs were higher than that of ML, which may explain that the grafting of amino-silane improves the specific surface area owing to the polycondensation of amino-silane (Lu 2013; Budnyak *et al.* 2018).

Operational Parameters of the Metal Ion Adsorption

To evaluate the adsorption ability of the ALs for Cd(II) and Pb(II), the effects of the AL dosage, pH, and setting time were investigated. The detailed experimental method is provided in the Appendix (Supplementary Information, *S1. Adsorption experiments*).

The dosage is a vital parameter for determining the adsorption capacity of ALs (Yu *et al.* 2021). The amounts of Cd(II) and Pb(II) ions removed at different adsorbent dosages are presented in Figs. 2(a) and (b), respectively. The removal efficiency of metal ions increased with the increasing adsorbent dosage, suggesting that increasing the adsorbent dosage resulted in a better removal efficiency owing to the interaction between the adsorbent particles and adsorbates with more active sites or surface area (Li *et al.* 2003a). Notably, the removal efficiency of metal ions onto PAL was higher than that of SAL and TAL. Moreover, the ALs exhibited better adsorption abilities for Pb(II) ions than for Cd(II) ions. To compare the adsorption abilities of the ALs, the amount of adsorbent that resulted in a heavy metal removal efficiency of approximately 98% was regarded as the optimal dosage for further adsorption experiments.

The role of pH in the adsorption ability of an adsorbent is one of the noteworthy in the adsorption experiments. In addition, its impacts on the ionization degree and surface charge of the functional groups on the active sites of adsorbent and adsorbate are very important (Shahabuddin *et al.* 2018; Murthy *et al.* 2020). The adsorption capacities of Cd(II) and Pb(II) ions at different pH values are shown in Figs. 2(c) and (d), respectively. The adsorption capacities of both Cd(II) and Pb(II) ions by ALs increased with an increase in pH. The adsorption capacities of ALs were poor for both heavy metals at pH 2.0 to 3.0. The protonation of ALs in an acidic environment caused the formation of cationic ammonium groups, resulting in the strong repulsion between ALs and cationic heavy metal ions (Li *et al.* 2019a). In contrast, under neutral conditions, ALs have a relatively good adsorption capacity of cationic heavy metal ions, which are expected to chelate with heavy metal cations because of the presence of lone pair electrons in ALs (Xu *et al.* 2016). Moreover, PAL exhibits a relatively high density of amine groups in the form of multilayered primary amine groups (Heo *et al.* 2022), suggesting that PAL has the highest ability to adsorb heavy metals. This can be explained by the relatively high number of active sites that can chelate with heavy metal ions. In addition, metal ions tend to form precipitates at high pH values, as shown in Fig. S2. When the pH exceeds 8, cadmium hydroxide is formed and cadmium is precipitated, and when the pH exceeds 7, lead precipitates due to the formation of lead hydroxide. Therefore, to simulate the optimization conditions, the adsorption experiments of Cd(II) and Pb(II) were conducted at pH 6.0 and 5.0, respectively.

The setting time provides an evaluation of the adsorbent properties between the adsorbent and adsorbate in the adsorption process. The Cd(II) and Pb(II) ion adsorption

capacities for ALs at various setting times in the range of 0 to 1440 min are presented in Figs. 2(e) and (f), respectively. With an increase in the contact time from 0 to 160 min, the adsorption capacities of the ALs increased rapidly at first, followed by a gradual increase, and they reached equilibrium after 1080 min. This trend shows that the adsorption capacities of metal ions onto the ALs increased with increasing setting time until the adsorption sites were fully occupied and equilibrium was attained (Qin *et al.* 2017). For the adsorption of Cd(II) ions, the equilibrium adsorption capacities of PAL, SAL, and TAL were 28.92, 19.3, and 11.8 mg·g⁻¹, respectively. For the adsorption of Pb(II) ions, the equilibrium adsorption capacities of PAL, SAL, and TAL were found to be 112.6, 39.8, and 38.9 mg·g⁻¹, respectively. These results indicate that the ALs have a higher binding affinity for Pb(II) than for Cd(II).

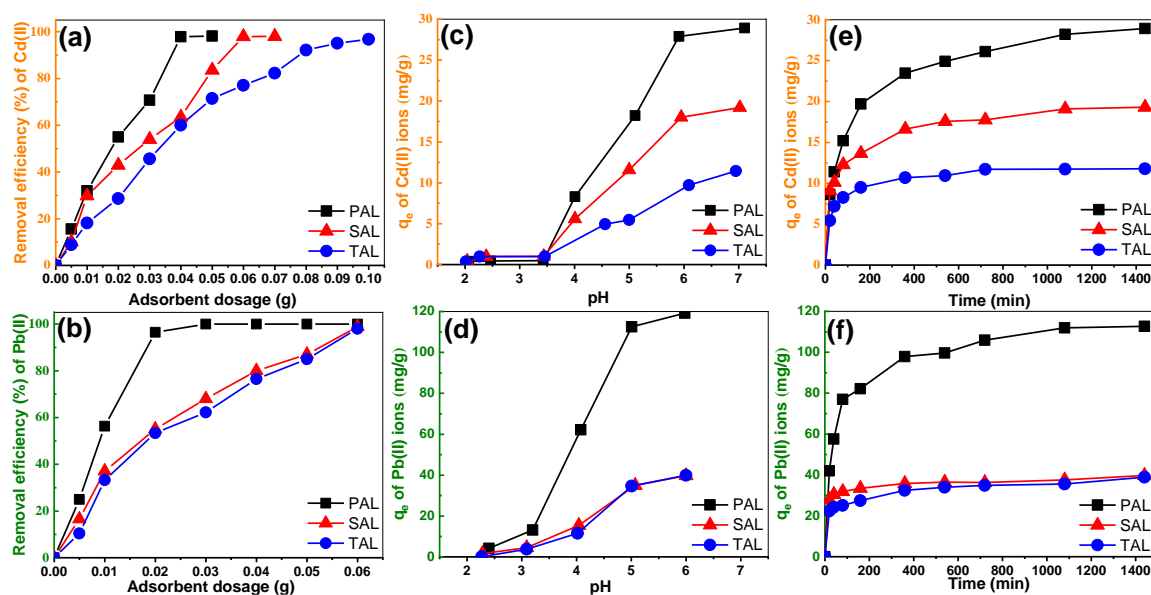


Fig. 2. Effect of the adsorbent dosage on the removal efficiency of (a) Cd(II) and (b) Pb(II) ions; effect of pH on the removal efficiency of (c) Cd(II) and (d) Pb(II) ions; effect of the setting time on the removal efficiency of (e) Cd(II) and (f) Pb(II) ions

Adsorption Kinetics

Adsorption kinetics indicate the rate of the adsorption process, which is important for interpreting the kinetic parameters of the adsorbents (Xu *et al.* 2016; Zhang *et al.* 2020a). The kinetic parameters were interpreted using pseudo-first-order (PFO) and pseudo-second-order (PSO) kinetic, as shown in Eqs. 3 and 4, respectively,

$$\ln(q_e - q_t) = \ln(q_e) - k_1 t, \quad (3)$$

$$t/q_t = 1/(k_2 \cdot q_e^2) + t/q_e, \quad (4)$$

where q_e is the equilibrium adsorption capacity (mg·g⁻¹), q_t is the adsorption capacity (mg·g⁻¹) at time t (min), and k_1 and k_2 are the kinetic rate constants of the PFO and PSO kinetic models, respectively.

The error percentage was interpreted using Eq. 5.

$$\text{Error percentage (\%)} = (q_{e(cal)} - q_{e(exp)}) / (q_{e(exp)}) \times 100, \quad (5)$$

Based on the experimental data (Figs. 2(e) and (f)) obtained from the analysis of

effects of the setting time on the removal rate, the PFO and PSO kinetic models were used to fit the data, and the results are presented in Fig. 3. The characteristic kinetic equation parameters are listed in Table 1.

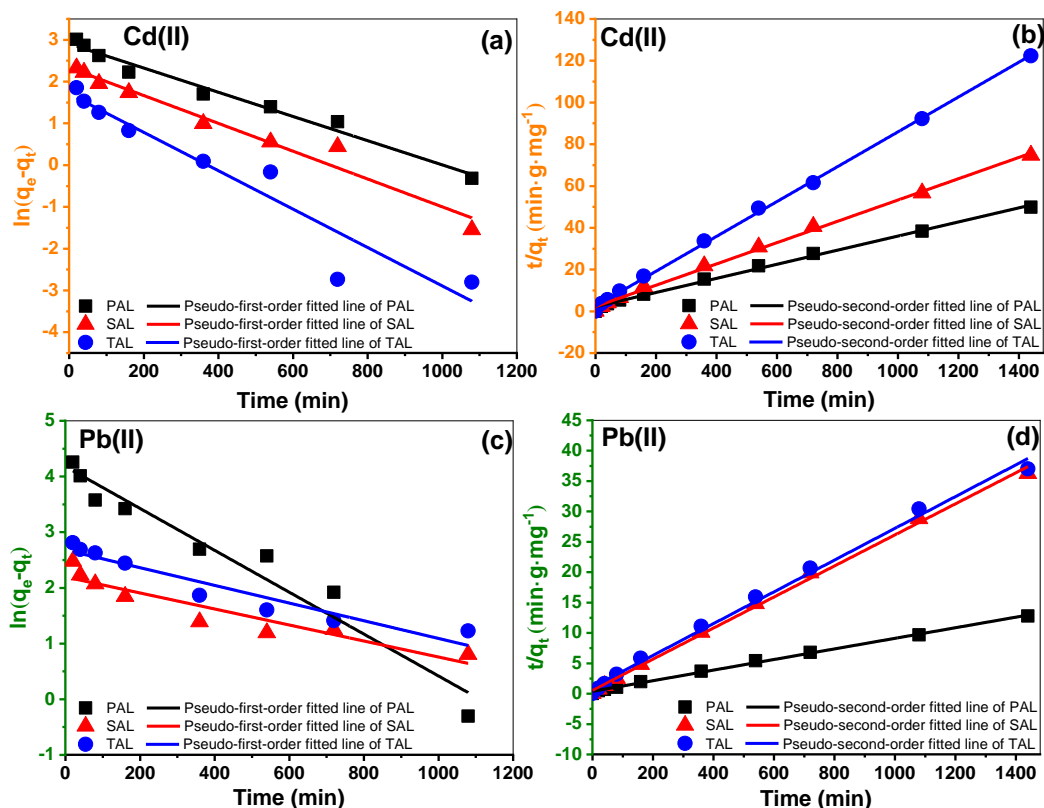


Fig. 3. Linear fitting curves of the PFO and PSO adsorption kinetic models for the adsorption of Cd(II) and Pb(II) ions onto ALs

Table 1. Characteristic Parameters of PFO and PSO Kinetics for the Adsorption of Cd(II) and Pb(II) Ions onto ALs

Isotherms	Parameters	Cd(II)			Pb(II)		
		PAL	SAL	TAL	PAL	SAL	TAL
Experimental data	$q_{e(exp)}$ (mg·g ⁻¹)	28.92	19.30	11.78	112.64	39.76	38.93
PFO kinetics	R ²	0.981	0.869	0.739	0.952	0.879	0.918
	k ₁ (min ⁻¹)	0.0029	0.003	0.0046	0.0038	0.0014	0.0016
	$q_{e(cal)}$ (mg·g ⁻¹)	18.21	10.28	5.49	65.16	8.97	14.56
	Error percent (%)	-37.03	-46.74	-53.40	-42.15	-77.44	-62.60
PSO kinetics	R ²	0.996	0.998	0.999	0.998	0.998	0.995
	k ₂ (g·mg ⁻¹ ·min ⁻¹)	0.0005	0.0510	0.0029	0.0002	0.0012	0.0006
	$q_{e(cal)}$ (mg·g ⁻¹)	29.60	19.60	11.98	114.68	39.11	38.26
	Error percent (%)	2.35	1.55	1.70	1.81	-1.63	-1.72

For the adsorption of both Cd(II) and Pb(II) ions, the q_e values calculated using the PSO kinetic model ($q_{e(cal)}$) were in good agreement with the experimental values ($q_{e(exp)}$). The error percentage of PSO kinetics was smaller than that of PFO kinetics. For all heavy metal ion adsorption processes, the coefficients of determination R^2 for the PSO kinetic models ($R^2 \geq 0.995$) were higher and closer to 1 than those for the PFO kinetic models ($R^2 \leq 0.981$). Therefore, the adsorption of Cd(II) and Pb(II) ions onto the ALs followed the PSO kinetic models, suggesting that the adsorption process involves diffusion of ions into narrow pores as the rate-limiting step (Hubbe *et al.* 2019)

Adsorption Equilibrium Isotherms

Adsorption isotherm studies explore the adsorption properties of materials and provide important data to determine whether the ALs can be used as adsorbents (Zhang *et al.* 2019a). The isotherm uptake parameters were analyzed using the Langmuir, Temkin, and Freundlich isotherms, which are given by Eqs. 6, 7, and 8, respectively,

$$C_e/q_e = 1/(q_{max} \cdot k_L) + C_e/q_{max}, \quad (6)$$

$$q_e/q_{max} = B \cdot \ln(k_T \cdot C_e), \quad (7)$$

$$\ln(q_e) = \ln(k_F) + \ln(C_e)/n, \quad (8)$$

where q_e is the equilibrium adsorption capacity ($\text{mg} \cdot \text{g}^{-1}$), C_e is the adsorbate concentration at equilibrium ($\text{mg} \cdot \text{L}^{-1}$), q_{max} is the maximum adsorption capacity ($\text{mg} \cdot \text{g}^{-1}$), k_L is the Langmuir constant, and $B = RT \cdot b_i^{-1}$ ($\text{kJ} \cdot \text{mol}^{-1}$), in which b_i ($\text{kJ} \cdot \text{mol}^{-1}$) and k_T ($\text{L} \cdot \text{mg}^{-1}$) are the Temkin constants related to the heat of adsorption and equilibrium binding constant, respectively. R ($8.314 \text{ J} \cdot \text{mol}^{-1} \cdot \text{K}^{-1}$) and T (K) are the universal gas constant and absolute solution temperature, respectively, whereas k_F and n are the Freundlich constants.

Figure S3 shows the effects of the initial adsorbate (Cd(II) and Pb(II)) concentrations on the adsorption capacity of PAL, SAL, and TAL. Figure 4 shows the experimental data fitted to the Langmuir, Temkin, and Freundlich isotherm equations, and the relevant linear equation parameters are summarized in Table 2. Based on the R^2 values, the experimental data for the Cd(II) and Pb(II) ions were well-fitted to the models in the following order: Langmuir > Temkin > Freundlich.

For the Langmuir isotherms, the dimensionless separation coefficient (R_L), which is an important characteristic of the Langmuir isotherm, was analyzed with Eq. 9,

$$R_L = 1 / (1 + k_L \cdot C_i), \quad (9)$$

where C_i ($\text{mg} \cdot \text{L}^{-1}$) is the initial dye concentration, and k_L ($\text{L} \cdot \text{mg}^{-1}$) is the Langmuir constant. Based on the R_L value, the isotherms can be classified as irreversible ($R_L = 0$), favorable ($0 < R_L < 1$), linear ($R_L = 1$), or unfavorable ($R_L > 1$) (Vargas *et al.* 2012; Wang *et al.* 2017). Therefore, the R_L values for all adsorption processes of metal ions are between 0 and 1, as listed in Table 2, which clearly indicate that metal ion adsorption on ALs *via* the monolayer coverage of metal ions was a favorable process.

The Temkin isotherm contains a factor that explicitly considers adsorbent–adsorbate interactions (Araújo *et al.* 2018). For Temkin isotherms, the b_i constant is related to the variation in the adsorption energy. The b_i values for the adsorption of Cd(II) ions onto PAL, SAL, and TAL were 19.6, 22.5, and 31.4 $\text{kJ} \cdot \text{mol}^{-1}$, respectively, whereas those for Pb(II) were 41.6, 49.0, and 54.3 $\text{kJ} \cdot \text{mol}^{-1}$, respectively. These results imply that all the adsorption processes were chemisorption because $b_i > 0.020 \text{ kJ} \cdot \text{mol}^{-1}$ (Araújo *et al.* 2018).

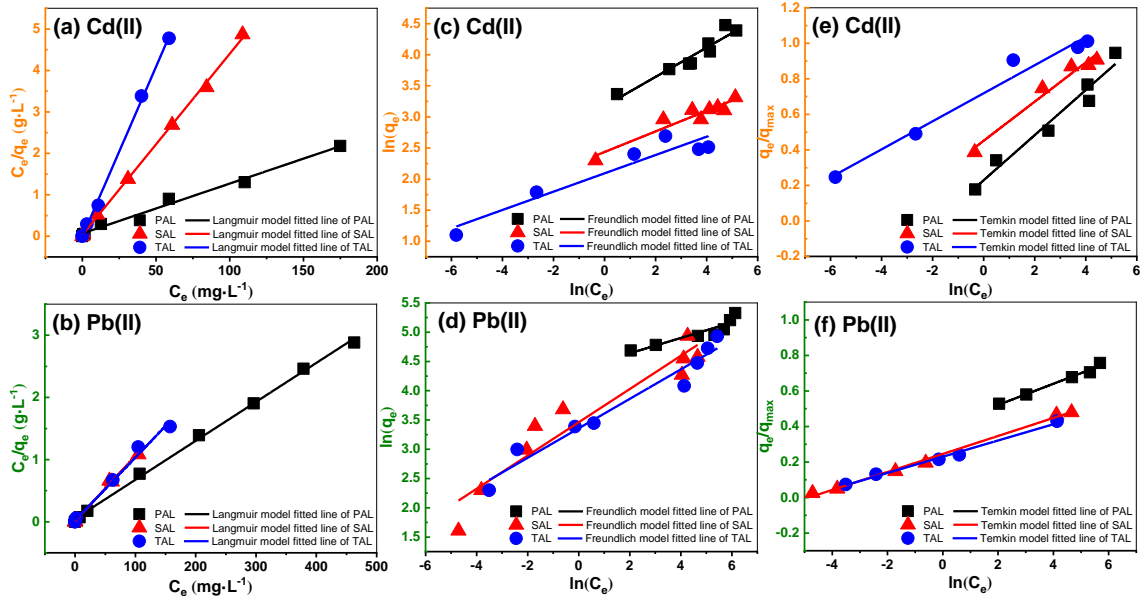


Fig. 4. Linear fitting curves of the adsorption isotherm models (Langmuir, Temkin, and Freundlich models) for the adsorption of Cd(II) and Pb(II) onto ALs

Table 2. Characteristic Parameters of Langmuir, Temkin, and Freundlich Models for the Adsorption of Cd(II) and Pb(II) Ions onto ALs

Isotherms	Parameters	Cd(II)			Pb(II)		
		PAL	SAL	TAL	PAL	SAL	TAL
Langmuir isotherm	R ²	0.991	0.999	0.999	0.998	0.997	0.992
	k _L (L·mg ⁻¹)	0.18	1.54	2.56	0.13	1.37	0.53
	q _{m(cal)} (mg·g ⁻¹)	83.19	22.88	12.20	159.74	95.42	98.72
	R _L	0.03-0.77	0.03-0.48	0.01-0.85	0.03-0.50	0.01-0.85	0.01-0.95
Temkin isotherm	R ²	0.963	0.970	0.976	0.985	0.995	0.992
	K _T (L·mg ⁻¹)	6.07	60.19	8953.93	830.79	125.74	151.10
	b _t (kJ·mol ⁻¹)	19.55	22.53	31.41	41.56	48.99	54.29
Freundlich isotherm	R ²	0.918	0.908	0.911	0.839	0.916	0.957
	k _F (mg·g ⁻¹)	23.85	11.41	8.10	79.55	31.78	28.67
	n	4.25	6.04	6.79	7.65	3.52	3.97

Adsorption Thermodynamics

Temperature is an important parameter that affects the mechanism and adsorption behavior of adsorbents (Shahabuddin *et al.* 2018; Zhang *et al.* 2019a). The thermodynamic studies were performed within the temperature range of 298.15 to 333.15 K. The data from the adsorption measured at various temperatures can be used to estimate thermodynamic parameters, such as changes in the standard free energy (ΔG°), enthalpy (ΔH°), and entropy (ΔS°) according to Eqs. 10, 11, and 12, respectively,

$$K_d = \lim_{C_e \rightarrow 0} q_e / C_e, \tag{10}$$

$$\Delta G^\circ = -RT \ln K_d, \quad (11)$$

$$\ln K_d = \frac{\Delta S^\circ}{R} - \frac{\Delta H^\circ}{R} \frac{1}{T}, \quad (12)$$

where K_d is the adsorption distribution coefficient, which was obtained by plotting $\ln(q_e/C_e)$ versus C_e at different temperatures and extrapolating to zero C_e , ΔH° is the standard enthalpy change ($\text{kJ}\cdot\text{mol}^{-1}$), ΔS° is the standard entropy change ($\text{J}\cdot\text{mol}^{-1}\cdot\text{K}^{-1}$), ΔG° is the standard free energy change ($\text{kJ}\cdot\text{mol}^{-1}$), R is the gas constant ($8.314 \text{ J}\cdot\text{mol}^{-1}\cdot\text{K}^{-1}$), and T is the absolute temperature (K).

Figure S4 shows the effects of temperature (298.2 to 333.2 K) on the adsorption capacity of the ALs for Cd(II) and Pb(II) ions. To evaluate the effects of temperature and sorption mechanism, a thermodynamic model based on Eqs. 10 to 12 was investigated. The thermodynamic parameters can be determined from the slope and intercept of the plot of $\ln(K_d)$ versus $1/T$ (Fig. 5). The details of the thermodynamic parameters are summarized in Table 3.

All ΔG° values for the metal ion adsorption were negative (Table 3), which demonstrates the feasibility and spontaneity of the process (Zhang *et al.* 2019a). The magnitude of the ΔG° values increased with increasing temperature, indicating that a better adsorption ability of ALs for metal ions was obtained at higher temperatures. The positive values of ΔH° and ΔS° of the ALs reflect an endothermic process and increased randomness in the sorption process (Table 3), respectively, which imply an increased affinity of the ALs for metal ions at higher temperatures (Popovic *et al.* 2020; Zhang *et al.* 2020b). The overall ΔS° values were positive because as the metal ions were adsorbed onto the surface of ALs, water molecules located around the metal ions in the solid–liquid interface were released into the solution (Shahabuddin *et al.* 2018).

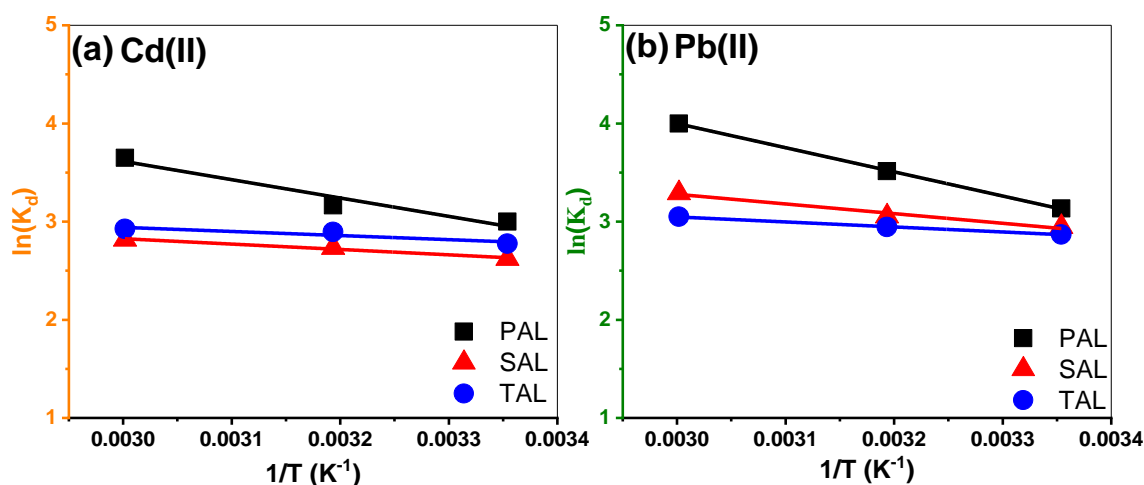


Fig. 5. Plots of $\ln(K_d)$ of ALs versus inverse temperature ($1/T$) for the adsorption of (a) Cd(II) and (b) Pb(II)

Table 3. Characteristic Parameters of Thermodynamic Studies for the Adsorption of Cd(II) and Pb(II) Ions onto ALs

Adsorbates	Samples	Parameter			
		Temperature (K)	ΔG° (kJ·mol ⁻¹)	ΔH° (kJ·mol ⁻¹)	ΔS° (J·mol ⁻¹ ·K ⁻¹)
Cd(II)	PAL	298.15	-7.44	15.55	76.69
		313.15	-8.24		
		333.15	-10.11		
	SAL	298.15	-6.50	4.55	37.15
		313.15	-7.12		
		333.15	-7.80		
	TAL	298.15	-6.88	3.47	34.87
		313.15	-7.53		
		333.15	-8.10		
Pb(II)	PAL	298.15	-7.77	20.46	94.63
		313.15	-9.15		
		333.15	-11.08		
	SAL	298.15	-7.31	8.18	51.81
		313.15	-7.95		
		333.15	-9.12		
	TAL	298.15	-7.11	4.24	37.89
		313.15	-7.66		
		333.15	-8.45		

Characterization of the Interaction between ALs and Heavy Metal Ions

To analyze the interactions with metal ions, the ALs were characterized before and after the adsorption of Cd(II) and Pb(II) *via* XPS. As shown in Fig. S5, the peaks of C 1s, O 1s, N 1s, and Si 2p were observed initially in the ALs. After the adsorption of metal ions, new clear peaks that correspond to Cd(II) and Pb(II) appeared in the XPS spectra of ALs-Cd(II) and ALs-Pb(II), respectively. These results indicate that Cd(II) and Pb(II) ions were successfully adsorbed onto the ALs. In addition, the core-level Cd 3d and Pb 4f spectra of PAL, SAL, and TAL after adsorption are illustrated in Fig. S6. After the Cd(II) adsorption, the core-level spectra showed two distinct peaks at approximately 404 and 411 eV, which were assigned to Cd 3d_{5/2} and Cd 3d_{3/2}, respectively (Chen *et al.* 2017; Peng *et al.* 2021). After the Pb(II) adsorption, the core-level spectra showed two clear peaks at approximately 137 and 142 eV, which were assigned to Pb 4f_{7/2} and Pb 4f_{5/2}, respectively (Li *et al.* 2019b). Figure 6 presents the N core-level spectra before and after metal ion adsorptions onto PAL, SAL, and TAL. After the adsorption of Cd(II) and Pb(II), the amine group (–NR₂) peaks shifted to 397.9 eV and 380 to 398.8 eV, respectively, whereas the protonated amine group (–NR₃⁺) peaks shifted to 399.7 to 400.6 eV and 400.0 to 400.6 eV, respectively, demonstrating the participation of the N-containing group in the metal ion adsorption processes (Li *et al.* 2019b; Heo *et al.* 2021). The lone pair of electrons in the N atoms was shared with Pb(II), leading to an increase in the binding energies (Xu *et al.* 2016). These results indicate that chemical interactions induce the adsorption of Cd(II) and Pb(II) onto ALs.

This adsorption mechanism can be explained using Pearson's hard/soft acid/base (HSAB) theory, where Cd(II) and Pb(II) are considered Lewis soft acids that tend to react with Lewis soft bases, such as amine groups of ALs (Xu *et al.* 2016; Jin *et al.* 2017). Electrostatic interaction and chelation occurred between the metal ions and ALs, which led to changes in the N electronic environment (Zhang *et al.* 2020b). This is further evidence

that the binding mechanism mainly proceeds through chelation mechanisms owing to the preference of Cd(II) and Pb(II) for amine groups.

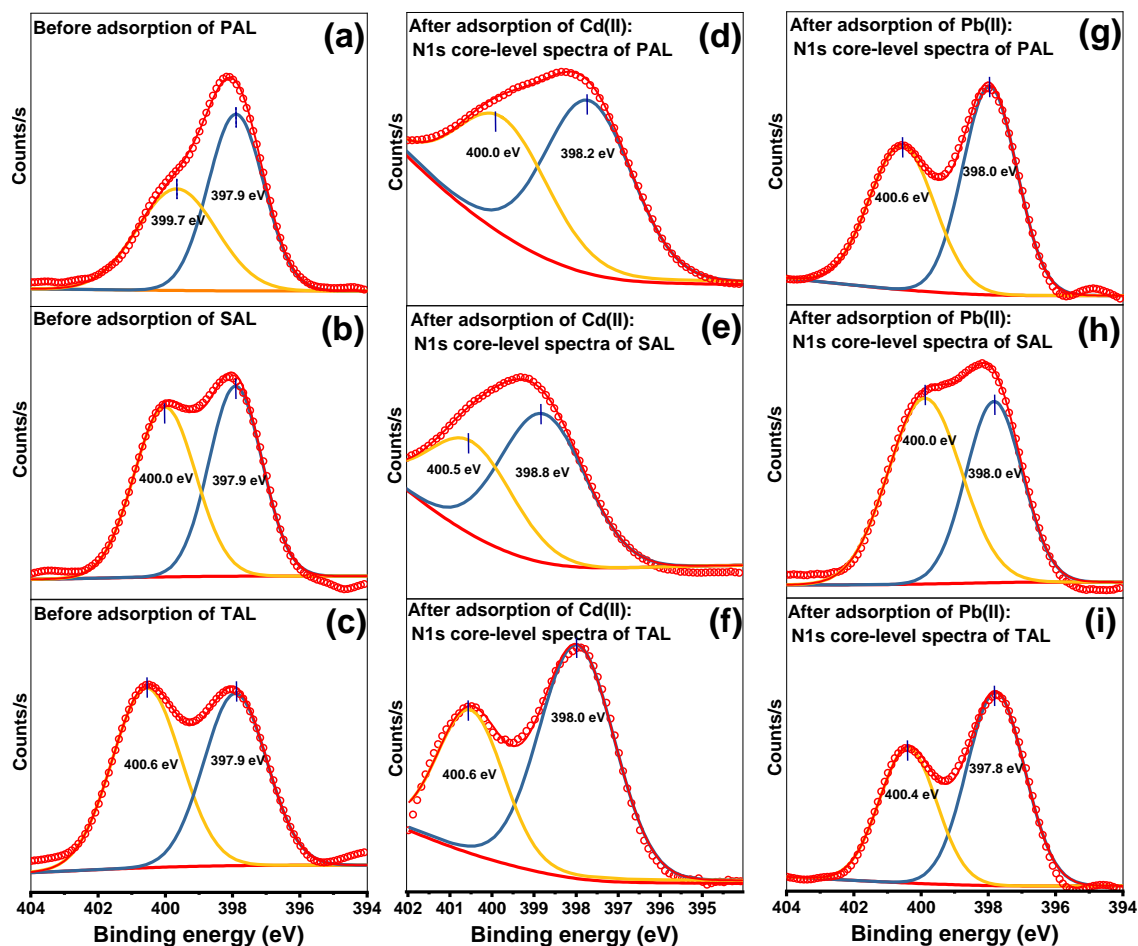


Fig. 6. N 1s core-level spectra of (a) PAL, (b) SAL, and (c) TAL before the adsorption; N 1s core-level spectra after the adsorption of Cd(II) onto (d) PAL, (e) SAL, and (f) TAL; N 1s core-level spectra after the adsorption of Pb(II) onto (g) PAL, (h) SAL, and (i) TAL

The FT-IR spectra (Fig. 7) of the ALs show the difference before and after metal ion adsorptions. The broad peaks at approximately 3400 and 3170 cm^{-1} were attributed to hydroxyl ($-\text{OH}$) and amine ($-\text{NR}_2$) groups, respectively (An *et al.* 2020; Popovic *et al.* 2020; Chen *et al.* 2021). In addition, the peak at 1100 cm^{-1} was assigned to Si–O, C–N, and C–O–C bonding, while the peak at 1030 cm^{-1} was assigned to Si–O–Si and C–O bonding (Li *et al.* 2019a; Heo *et al.* 2022). The peaks at 737 and 693 cm^{-1} were assigned to Si–C and Si–O–Si, respectively (Heo *et al.* 2022). However, after metal ion adsorption, slightly different absorption peaks were observed.

After metal ion adsorption, peaks were observed at 3400 , 1662 , 1265 , 1215 , 1150 , 737 , and 693 cm^{-1} . The peaks at approximately 3400 cm^{-1} (hydroxyl group) were stronger than those of the ALs before adsorption. In addition, the peak at 3170 cm^{-1} after metal ion adsorption indicates the presence of amine groups, whereas the peaks at 1265 , 1215 , and 1150 cm^{-1} were broader and stronger. Significantly, a new peak at 1662 cm^{-1} was observed, corresponding to amine group bending (Li *et al.* 2019b). This can be explained by the interaction between the amine groups of the ALs and the metal ions (Xu *et al.* 2016). In

contrast, the peaks at 737 and 693 cm^{-1} disappeared, indicating that the strength of the hydroxyl group increased, and the peaks disappeared because the structure of ALs changed because of the interconversion of siloxane to silanol *via* hydration (Warring *et al.* 2016). It could be suggested that an increase in silanol may participate in the interaction with metal ions (Li *et al.* 2020). Therefore, owing to the shift and intensity changes of the amine and hydroxyl groups, these two groups were established as the main functional groups that interact with the metal ions (Lei *et al.* 2019).

The morphologies of the ALs before and after the adsorption are shown in Fig. S7. After adsorption of Cd(II) and Pb(II), many metal ion particles were adsorbed on the surface of ALs. According to Heo *et al.* (2022), the Brunauer–Emmett–Teller surface analysis confirmed that ALs have a mesoporous structure, implying that the metal ion adsorption capacity of ALs was enhanced owing to the presence of exposed specific surface area and pore. In addition, Table S2 shows the surface atomic content of the ALs after Cd(II) and Pb(II) adsorptions. After the adsorption of metal ions, Cd(II) and Pb(II) appeared on the surface of the ALs, suggesting the successful adsorption of the metal ions. In this study, PAL exhibited the highest adsorption ability for metal ions among the ALs.

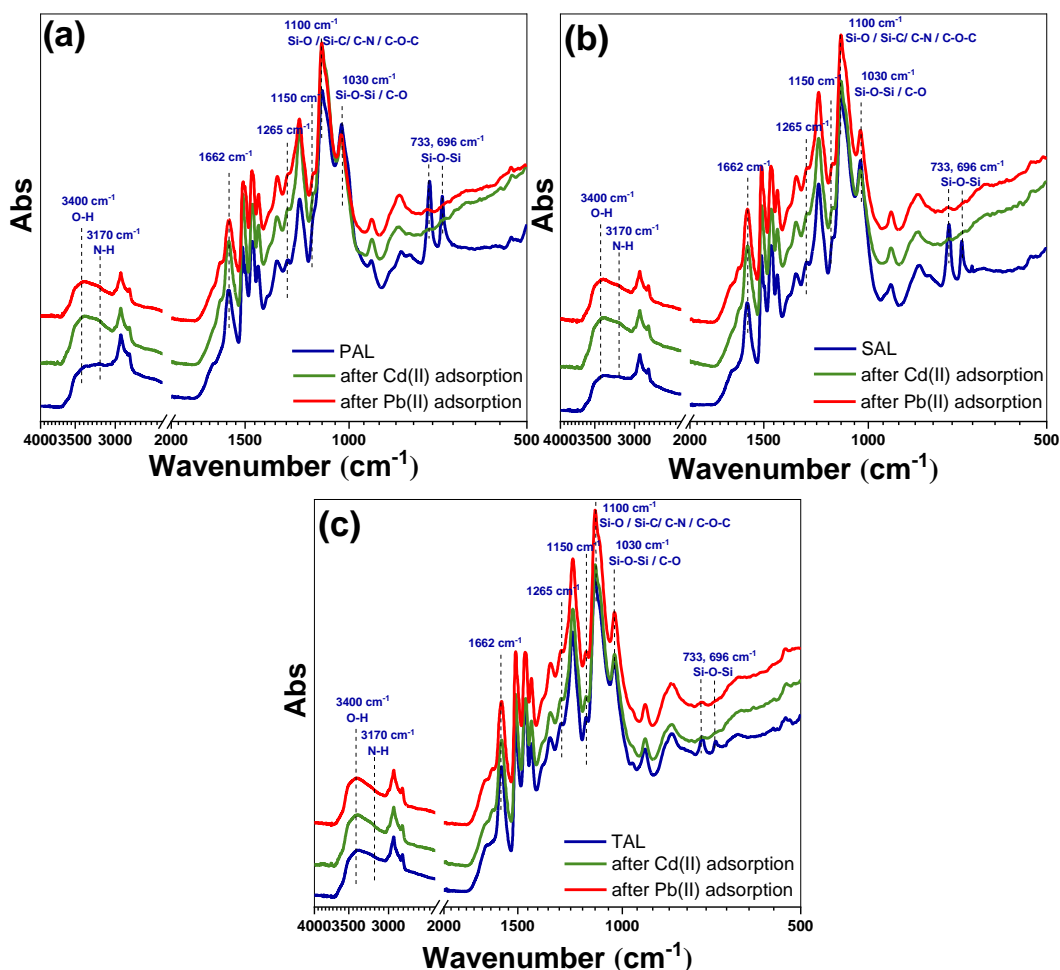


Fig. 7. FT-IR spectra of (a) PAL, (b) SAL, and (c) TAL before and after metal ion adsorptions

Adsorption Mechanism of Cd(II) and Pb(II) Ions

The heavy metal ion adsorption behaviors of the AL adsorbents were compared with those of other reported modified lignin-based adsorbents, as summarized in Table 4 (Peternele *et al.* 1999; Ge *et al.* 2014; Klapiszewski *et al.* 2015; Jin *et al.* 2017; Klapiszewski *et al.* 2017; Zhou *et al.* 2021). The maximum Cd(II) and Pb(II) adsorption capacity values of PAL were 83.19 and 159.7 mg·g⁻¹, respectively, which are higher than those of the recently reported modified lignin-based adsorbents. This superior adsorption behavior of PAL is attributed to the presence of many hydroxyl and amine groups (active sites) provided by the amino-silane grafted on the lignin surface. The presence of lone pair electrons in the O- and N-containing groups, which enable chelation with metal ions, explains the superior behavior of PAL for the adsorption of Cd(II) and Pb(II).

Table 4. Comparison of q_e of the ALs for Cd(II) and Pb(II) Metal Ions with Other Modified Lignin-Based Adsorbents

Adsorbate	Adsorbent	q_e (mg·g ⁻¹)	Reference
Cd(II)	Lignin cane carboxymethylation	67.7	(Peternele <i>et al.</i> 1999)
	Lignin (bamboo) modification <i>via</i> thiol-yne	72.4	(Jin <i>et al.</i> 2017)
	Amino-functionalized lignin microspheres	74.8	(Popovic <i>et al.</i> 2020)
	Silica-kraft lignin composite	84.7	(Klapiszewski <i>et al.</i> 2015)
	Primary aminated lignin (PAL)	83.2	This work
	Secondary aminated lignin (SAL)	22.9	This work
	Tertiary aminated lignin (TAL)	12.2	This work
Pb(II)	Alkaline lignin-sulfomethylation and amination	53.8	(Ge <i>et al.</i> 2014)
	TiO ₂ -SiO ₂ /lignin hybrid	59.9	(Klapiszewski <i>et al.</i> 2017)
	Aminated epoxy-lignin	72.5	(Liu <i>et al.</i> 2013)
	Lignin cane carboxyl methylation	107.5	(Peternele <i>et al.</i> 1999)
	lignin-based magnetic adsorbent	111.2	(Zhou <i>et al.</i> 2021)
	Primary aminated lignin (PAL)	159.7	This work
	Secondary aminated lignin (SAL)	95.4	This work
	Tertiary aminated lignin (TAL)	98.7	This work

Notably, the ALs showed higher adsorption capacity for Pb(II) ions than for Cd(II) ions. In particular, some studies have reported that Pb(II) ions have a greater chelating capacity with amine groups than Cd(II) ions (Xu *et al.* 2016; Heo *et al.* 2021; Zhou *et al.* 2021). This suggests that in the acid/base classification, the metal can be ranked as borderline (Pb(II)) and soft acid (Cd(II)), according to the HSAB theory (Zhou *et al.* 2021). Therefore, the chelating ability between the ALs and Pb(II) is superior to that between the ALs and Cd(II). Moreover, the adsorption mechanism involves the cation- π interaction between the positively charged metal ion and π -electron cloud of the negatively charged aromatic ring (Wang *et al.* 2020a; Zhao and Zhu 2020). Therefore, the synergistic effects of various interactions between metal ions and ALs, including the chelating, electrostatic,

and cation- π interactions, contribute to the adsorption process (Fig. 8) (Zhao and Zhu 2020). By introducing amino-silane into lignin, the ability of ALs to adsorb metal ions was improved by the inclusion of aromatic rings, amines, and hydroxyl groups in the structure of ALs.

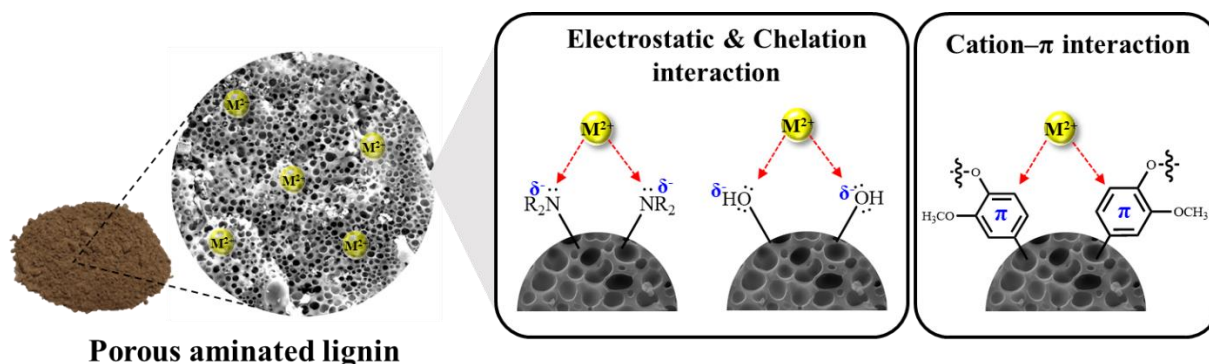


Fig. 8. Hypothetical adsorption mechanism of metal ions onto aminated lignin

CONCLUSIONS

1. ALs with primary, secondary, and tertiary amine groups were synthesized through one-step modification using three types of amino-silane reagents and applied to adsorb heavy metal ions.
2. The ALs exhibited optimal Cd(II) and Pb(II) adsorption capacities in a neutral environment, where the attraction between the lone pair electrons of ALs and the cationic Cd(II) and Pb(II) species was maximized.
3. The adsorption process followed Langmuir isotherms, suggesting that metal ions were adsorbed onto the ALs by forming a homogeneous monolayer. The maximum adsorption capacities for Cd(II) and Pb(II) ions were 83.2 and 159.7 mg·g⁻¹, respectively.
4. The attraction between the N- and O-containing groups in the ALs and cationic metal ions also plays a critical role in the adsorption.
5. This study presents bio-adsorbents for high-performance lignin-based adsorption for the removal of hazardous water pollutants.

ACKNOWLEDGMENTS

This work was supported by the National Research Foundation of Korea (NRF) grant funded by the Korea government (MSIT) (2021R1A2C2008178), and the Ministry of Education (2018R1A6A1A03025582).

REFERENCES CITED

- An, L., Chen, J., Heo, J. W., Bae, J. H., Jeong, H., and Kim, Y. S. (2021). "Synthesis of lignin-modified cellulose nanocrystals with antioxidant activity *via* Diels–Alder reaction and its application in carboxymethyl cellulose film," *Carbohydr. Polym.* 274, 118651. DOI: 10.1016/j.carbpol.2021.118651
- An, L., Si, C., Bae, J. H., Jeong, H., and Kim, Y. S. (2020). "One-step silanization and amination of lignin and its adsorption of Congo red and Cu (II) ions in aqueous solution," *Int. J. Biol. Macromol.* 159, 222-230. DOI: 10.1016/j.ijbiomac.2020.05.072
- Araújo, C. S., Almeida, I. L., Rezende, H. C., Marcionilio, S. M., Léon, J. J., and de Matos, T. N. (2018). "Elucidation of mechanism involved in adsorption of Pb (II) onto lobeira fruit (*Solanum lycocarpum*) using Langmuir, Freundlich and Temkin isotherms," *Microchem.* 137, 348-354. DOI: 10.1016/j.microc.2017.11.009.
- Awaleh, M. O., and Soubaneh, Y. D. (2014). "Waste water treatment in chemical industries: the concept and current technologies," *Hydrol. Curr. Res.* 5(1), 1. DOI: 10.4172/2157-7587.1000164
- Bian, Y., Bian, Z., Zhang, J., Ding, A., Liu, S., Zheng, L., and Wang, H. (2015). "Adsorption of cadmium ions from aqueous solutions by activated carbon with oxygen-containing functional groups," *Chin. J. Chem. Eng.* 23(10), 1705-1711. DOI: 10.1016/j.cjche.2015.08.031
- Boamah, P. O., Huang, Y., Hua, M., Zhang, Q., Wu, J., Onumah, J., Sam-Amoah, L. K., and Boamah, P. O. (2015). "Sorption of heavy metal ions onto carboxylate chitosan derivatives—a mini-review," *Ecotoxicol. Environ. Saf.* 116, 113-120. DOI: 10.1016/j.ecoenv.2015.01.012
- Boparai, H. K., Joseph, M., and O'Carroll, D. M. (2013). "Cadmium (Cd²⁺) removal by nano zerovalent iron: Surface analysis, effects of solution chemistry and surface complexation modeling," *Environ. Sci. Pollut. Res.* 20(9), 6210-6221. DOI: 10.1007/s11356-013-1651-8
- Budnyak, T. M., Aminzadeh, S., Pylypchuk, I. V., Sternik, D., Tertykh, V. A., Lindström, M. E., and Sevastyanova, O. (2018). "Methylene Blue dye sorption by hybrid materials from technical lignins," *J. Environ. Chem. Eng.* 6(4), 4997-5007. DOI: 10.1016/j.jece.2018.07.041
- Chen, G., Shah, K. J., Shi, L., and Chiang, P.-C. (2017). "Removal of Cd (II) and Pb (II) ions from aqueous solutions by synthetic mineral adsorbent: performance and mechanisms," *Appl. Surf. Sci.* 409, 296-305. DOI: 10.1016/j.apsusc.2017.03.022.
- Chen, J., An, L., Bae, J. H., Heo, J. W., Han, S. Y., and Kim, Y. S. (2021). "Green and facile synthesis of aminated lignin-silver complex and its antibacterial activity," *Ind Crops Prod.* 173, 114102. DOI: 10.1016/j.indcrop.2021.114102
- Duan, Y., Freyburger, A., Kunz, W., and Zollfrank, C. (2018). "Lignin/chitin films and their adsorption characteristics for heavy metal ions," *ACS Sustain. Chem. Eng.* 6(5), 6965-6973. DOI: 10.1021/acssuschemeng.8b00805
- Dutta, K., Mukhopadhyay, S., Bhattacharjee, S., and Chaudhuri, B. (2001). "Chemical oxidation of methylene blue using a Fenton-like reaction," *J. Hazard. Mater.* 84(1), 57-71. DOI: 10.1016/S0304-3894(01)00202-3
- Gaur, V. K., Gupta, S. K., Pandey, S., Gopal, K., and Misra, V. (2005). "Distribution of heavy metals in sediment and water of river Gomti," *Environ. Monit. Assess.* 102(1), 419-433. DOI: 10.1007/s10661-005-6395-6
- Gdula, K., Gładysz-Płaska, A., Cristovao, B., Ferenc, W., and Skwarek, E. (2019).

- "Amine-functionalized magnetite-silica nanoparticles as effective adsorbent for removal of uranium (VI) ions," *J. Mol. Liq.* 290, article no. 111217. DOI: 10.1016/j.molliq.2019.111217
- Ge, Y., Li, Z., Kong, Y., Song, Q., and Wang, K. (2014). "Heavy metal ions retention by bi-functionalized lignin: Synthesis, applications, and adsorption mechanisms," *J. Ind. Eng. Chem.* 20(6), 4429-4436. DOI: 10.1016/j.jiec.2014.02.011
- Genchi, G., Sinicropi, M. S., Lauria, G., Carocci, A., and Catalano, A. (2020). "The effects of cadmium toxicity," *Int. J. Environ. Res. Public Health* 17(11), 3782. DOI: 10.3390/ijerph17113782
- Gocht, T., Moldenhauer, K.-M., and Püttmann, W. (2001). "Historical record of polycyclic aromatic hydrocarbons (PAH) and heavy metals in floodplain sediments from the Rhine River (Hessisches Ried, Germany)," *Appl. Geochem.* 16(15), 1707-1721. DOI: 10.1016/S0883-2927(01)00063-4
- Guibal, E. (2004). "Interactions of metal ions with chitosan-based sorbents: A review," *Sep. Purif. Technol.* 38(1), 43-74. DOI: 10.1016/j.seppur.2003.10.004
- He, Y., Li, G., Wang, H., Zhao, J., Su, H., and Huang, Q. (2008). "Effect of operating conditions on separation performance of reactive dye solution with membrane process," *J. Membr. Sci.* 321(2), 183-189. DOI: 10.1016/j.memsci.2008.04.056
- Heo, J. W., An, L., Chen, J., Bae, J. H., and Kim, Y. S. (2022). "Preparation of amine-functionalized lignins for the selective adsorption of Methylene blue and Congo red," *Chemosphere* article no. 133815. DOI: 10.1016/j.chemosphere.2022.133815
- Heo, J. W., Kim, M. S., Kim, M. J., and Kim, Y. S. (2021). "Synthesis of di-amine functionalized lignin derivative and its removal ability for heavy metal ions," *Palpu Chongi Gisul/J. Korea Tech. Assoc. Pulp Pap. Ind.* 53(6), 85-97. DOI: 10.7584/JKTAPPI.2021.12.53.6.85
- Hubbe, M. A., Azizian, S., and Douven, S. (2019). "Implications of apparent pseudo-second-order adsorption kinetics onto cellulosic materials. A review," *BioResources* 14(3), 7582-7626. DOI: 10.15376/biores.14.3.7582-7626
- Jin, C., Zhang, X., Xin, J., Liu, G., Wu, G., Kong, Z., and Zhang, J. (2017). "Clickable synthesis of 1, 2, 4-triazole modified lignin-based adsorbent for the selective removal of Cd (II)," *ACS Sustain. Chem. Eng.* 5(5), 4086-4093. DOI: 10.1021/acssuschemeng.7b00072
- Kadirvelu, K., Kavipriya, M., Karthika, C., Radhika, M., Vennilamani, N., and Pattabhi, S. (2003). "Utilization of various agricultural wastes for activated carbon preparation and application for the removal of dyes and metal ions from aqueous solutions," *Bioresour. Technol.* 87(1), 129-132. DOI: 10.1016/S0960-8524(02)00201-8
- Klapiszewski, Ł., Bartczak, P., Wysokowski, M., Jankowska, M., Kabat, K., and Jesionowski, T. (2015). "Silica conjugated with kraft lignin and its use as a novel 'green' sorbent for hazardous metal ions removal," *Chem. Eng. J.* 260, 684-693. DOI: 10.1016/j.cej.2014.09.054
- Klapiszewski, Ł., Siwińska-Stefańska, K., and Kołodyńska, D. (2017). "Preparation and characterization of novel TiO₂/lignin and TiO₂-SiO₂/lignin hybrids and their use as functional biosorbents for Pb (II)," *Chem. Eng. J.* 314, 169-181. DOI: 10.1016/j.cej.2016.12.114
- Kyzas, G. Z., and Kostoglou, M. (2014). "Green adsorbents for wastewaters: A critical review," *Materials*, 7(1), 333-364. DOI: 10.3390/ma7010333
- Lei, T., Li, S.-J., Jiang, F., Ren, Z.-X., Wang, L.-L., Yang, X.-J., Tang, L.-H., and Wang, S.-X. (2019). "Adsorption of cadmium ions from an aqueous solution on a highly

- stable dopamine-modified magnetic nano-adsorbent,” *Nanoscale Res. Lett.* 14(1), 1-17. DOI: 10.1186/s11671-019-3154-0
- Li, P., Wang, J., Li, X., Zhu, W., He, S., Han, C., Luo, Y., Ma, W., Liu, N., and Dionysiou, D. D. (2019a). "Facile synthesis of amino-functional large-size mesoporous silica sphere and its application for Pb²⁺ removal,” *J. Hazard. Mater.* 378, article no. 120664. DOI: 10.1016/j.jhazmat.2019.05.057
- Li, Y.-H., Ding, J., Luan, Z., Di, Z., Zhu, Y., Xu, C., Wu, D., and Wei, B. (2003a). "Competitive adsorption of Pb²⁺, Cu²⁺ and Cd²⁺ ions from aqueous solutions by multiwalled carbon nanotubes,” *Carbon* 41(14), 2787-2792. DOI: 10.1016/S0008-6223(03)00392-0
- Li, Y.-H., Wang, S., Luan, Z., Ding, J., Xu, C., and Wu, D. (2003b). "Adsorption of cadmium (II) from aqueous solution by surface oxidized carbon nanotubes,” *Carbon* 41(5), 1057-1062. DOI: 10.1016/S0008-6223(02)00440-2
- Li, Z., Pan, Z., and Wang, Y. (2019b). "Enhanced adsorption of cationic Pb (II) and anionic Cr (VI) ions in aqueous solution by amino-modified nano-sized illite-smectite clay,” *Environ. Sci. Pollut. Res.* 26(11), 11126-11139. DOI: 10.1007/s11356-019-04447-0
- Li, Z., Pan, Z., and Wang, Y. (2020). "Preparation of ternary amino-functionalized magnetic nano-sized illite-smectite clay for adsorption of Pb (II) ions in aqueous solution,” *Environ. Sci. Pollut. Res.* 1-14. DOI: 10.1007/s11356-020-07766-9
- Liu, W., Yang, L., Xu, S., Chen, Y., Liu, B., Li, Z., and Jiang, C. (2018). "Efficient removal of hexavalent chromium from water by an adsorption–reduction mechanism with sandwiched nanocomposites,” *RSC Adv.* 8(27), 15087-15093. DOI: 10.1039/C8RA01805G
- Liu, X., Zhu, H., Qin, C., Zhou, J., Zhao, J. R., and Wang, S. (2013). “Adsorption of heavy metal ion from aqueous single metal solution by aminated epoxy-lignin,” *BioResources* 8(2), 2257-2269.
- Lora, J. H., and Glasser, W. G. (2002). "Recent industrial applications of lignin: A sustainable alternative to nonrenewable materials,” *J. Polym. Environ.* 10(1), 39-48. DOI: 10.1023/A:1021070006895
- Lu, H.-T. (2013). "Synthesis and characterization of amino-functionalized silica nanoparticles,” *Colloid Journal* 75(3), 311-318. DOI: 10.1134/S1061933X13030125
- Murthy, T. K., Gowrishankar, B., Krishna, R. H., Chandraprabha, M., and Mathew, B. B. (2020). "Magnetic modification of coffee husk hydrochar for adsorptive removal of methylene blue: isotherms, kinetics and thermodynamic studies,” *Environmental Chemistry and Ecotoxicology* 2, 205-212. DOI: 10.1016/j.enceco.2020.10.002
- Peng, Z.-d., Lin, X.-m., Zhang, Y.-l., Hu, Z., Yang, X.-j., Chen, C.-y., Chen, H.-y., Li, Y.-t., and Wang, J.-j. (2021). "Removal of cadmium from wastewater by magnetic zeolite synthesized from natural, low-grade molybdenum,” *Sci. Total Environ.* 772, article no. 145355. DOI: 10.1016/j.scitotenv.2021.145355
- Peternele, W. S., Winkler-Hechenleitner, A. A., and Pineda, E. A. G. (1999). “Adsorption of Cd (II) and Pb (II) onto functionalized formic lignin from sugar cane bagasse,” *Bioresour. Technol.* 68(1), 95-100. DOI: 10.1016/S0960-8524(98)00083-2
- Popovic, A. L., Rusmirovic, J. D., Velickovic, Z., Radovanovic, Z., Ristic, M., Pavlovic, V. P., and Marinkovic, A. D. (2020). “Novel amino-functionalized lignin microspheres: High performance biosorbent with enhanced capacity for heavy metal ion removal,” *Int. J. Biol. Macromol.* 156, 1160-1173. DOI: 10.1016/j.ijbiomac.2019.11.152

- Pyrzynska, K. (2019). "Removal of cadmium from wastewaters with low-cost adsorbents," *J. Environ. Chem. Eng.* 7(1), article no. 102795. DOI: 10.1016/j.jece.2018.11.040.
- Qin, L., Ge, Y., Deng, B., and Li, Z. (2017). "Poly (ethylene imine) anchored lignin composite for heavy metals capturing in water," *J. Taiwan Inst. Chem. Engrs.* 71, 84-90. DOI: 10.1016/j.jtice.2016.11.012
- Santander, P., Butter, B., Oyarce, E., Yáñez, M., Xiao, L.-P., and Sánchez, J. (2021). "Lignin-based adsorbent materials for metal ion removal from wastewater: A review," *Ind. Crops Prod.* 167, article no. 113510. DOI: 10.1016/j.indcrop.2021.113510
- Sekar, M., Sakthi, V., and Rengaraj, S. (2004). "Kinetics and equilibrium adsorption study of lead (II) onto activated carbon prepared from coconut shell," *J. Colloid Interface Sci.* 279(2), 307-313. DOI: 10.1016/j.jcis.2004.06.042
- Shahabuddin, S., Tashakori, C., Kamboh, M. A., Korrani, Z. S., Saidur, R., Nodeh, H. R., and Bidhendi, M. E. (2018). "Kinetic and equilibrium adsorption of lead from water using magnetic metformin-substituted SBA-15," *Environ. Sci.: Water Res. Technol.* 4(4), 549-558. DOI: 10.1039/C7EW00552K
- Stafiej, A., and Pyrzynska, K. (2007). "Adsorption of heavy metal ions with carbon nanotubes," *Sep. Purif. Technol.* 58(1), 49-52. DOI: 10.1016/j.seppur.2007.07.008
- Vargas, A. M., Cazetta, A. L., Martins, A. C., Moraes, J. C., Garcia, E. E., Gauze, G. F., Costa, W. F., and Almeida, V. C. (2012). "Kinetic and equilibrium studies: Adsorption of food dyes Acid Yellow 6, Acid Yellow 23, and Acid Red 18 on activated carbon from flamboyant pods," *Chem. Eng. J.* 181, 243-250. DOI: 10.1016/j.cej.2011.11.073
- Wamba, A. G., Kofa, G. P., Koungou, S. N., Thue, P. S., Lima, E. C., dos Reis, G. S., and Kayem, J. G. (2018). "Grafting of amine functional group on silicate based material as adsorbent for water purification: A short review," *J. Environ. Chem. Eng.*, 6(2), 3192-3203. DOI: 10.1016/j.jece.2018.04.062
- Wang, F., Pan, Y., Cai, P., Guo, T., and Xiao, H. (2017). "Single and binary adsorption of heavy metal ions from aqueous solutions using sugarcane cellulose-based adsorbent," *Bioresour. Technol.* 241, 482-490. DOI: 10.1016/j.biortech.2017.05.162
- Wang, B., Sun, Y.-C., and Sun, R.-C. (2019). "Fractional and structural characterization of lignin and its modification as biosorbents for efficient removal of chromium from wastewater: A review," *J. Leather Sci. Eng.* 1(1), 1-25. DOI: 10.1186/s42825-019-0003-y
- Wang, B., Ran, M., Fang, G., Wu, T., and Ni, Y. (2020a). "Biochars from lignin-rich residue of furfural manufacturing process for heavy metal ions remediation," *Materials* 13(5), 1037. DOI: 10.3390/ma13051037
- Wang, Q., Zheng, C., Cui, W., He, F., Zhang, J., Zhang, T. C., and He, C. (2020b). "Adsorption of Pb²⁺ and Cu²⁺ ions on the CS₂-modified alkaline lignin," *Chem. Eng. J.* 391, article no. 123581. DOI: 10.1016/j.cej.2019.123581
- Warring, S. L., Beattie, D. A., and McQuillan, A. J. (2016). "Surficial siloxane-to-silanol interconversion during room-temperature hydration/dehydration of amorphous silica films observed by ATR-IR and TIR-Raman spectroscopy," *Langmuir*, 32(6), 1568-1576. DOI: 10.1021/acs.langmuir.5b04506
- Xu, G., Xie, Y., Cao, J., Tao, M., and Zhang, W.-Q. (2016). "Highly selective and efficient chelating fiber functionalized by bis (2-pyridylmethyl) amino group for heavy metal ions," *Polym. Chem.* 7(23), 3874-3883. DOI: 10.1039/C6PY00335D.

- Yu, Y. H., An, L., Bae, J. H., Heo, J. W., Chen, J., Jeong, H., and Kim, Y. S. (2021). "A novel biosorbent from hardwood cellulose nanofibrils grafted with poly (m-aminobenzene sulfonate) for adsorption of Cr (VI)," *Front. Bioeng. Biotechnol.* 9, 320. DOI: 10.3389/fbioe.2021.682070
- Zhang, D., Wang, L., Zeng, H., Rhimi, B., and Wang, C. (2020a). "Novel polyethyleneimine functionalized chitosan–lignin composite sponge with nanowall-network structures for fast and efficient removal of Hg (ii) ions from aqueous solution," *Environ. Sci. Nano* 7(3), 793-802. DOI: 10.1039/C9EN01368G
- Zhang, M., Yin, Q., Ji, X., Wang, F., Gao, X., and Zhao, M. (2020b). "High and fast adsorption of Cd (II) and Pb (II) ions from aqueous solutions by a waste biomass based hydrogel," *Sci. Rep.* 10(1), 1-13. DOI: 10.1038/s41598-020-60160-w
- Zhang, S., Shi, Q., Christodoulatos, C., and Meng, X. (2019a). "Lead and cadmium adsorption by electrospun PVA/PAA nanofibers: Batch, spectroscopic, and modeling study," *Chemosphere* 233, 405-413. DOI: 10.1016/j.chemosphere.2019.05.190
- Zhang, Y., Ni, S., Wang, X., Zhang, W., Lagerquist, L., Qin, M., Willför, S., Xu, C., and Fatehi, P. (2019b). "Ultrafast adsorption of heavy metal ions onto functionalized lignin-based hybrid magnetic nanoparticles," *Chem. Eng. J.* 372, 82-91. DOI: 10.1016/j.cej.2019.04.111
- Zhao, G., and Zhu, H. (2020). "Cation– π interactions in graphene-containing systems for water treatment and beyond," *Adv. Mater.* 32(22), article no. 1905756. DOI: 10.1002/adma.201905756
- Zhou, X., Jin, C., Liu, G., Wu, G., Huo, S., and Kong, Z. (2021). "Functionalized lignin-based magnetic adsorbents with tunable structure for the efficient and selective removal of Pb (II) from aqueous solution," *Chem. Eng. J.* article no. 130409. DOI: 10.1016/j.cej.2021.130409
- Zong, E., Huang, G., Liu, X., Lei, W., Jiang, S., Ma, Z., Wang, J., and Song, P. (2018). "A lignin-based nano-adsorbent for superfast and highly selective removal of phosphate," *J. Mater. Chem. A* 6(21), 9971-9983. DOI: 10.1039/C8TA01449C

Article submitted: June 16, 2022; Peer review completed: August 27, 2022; Revised version received and accepted: September 2, 2022; Published: September 8, 2022.
DOI: 10.15376/biores.17.4.5958-5983

APPENDIX

Supplementary Information

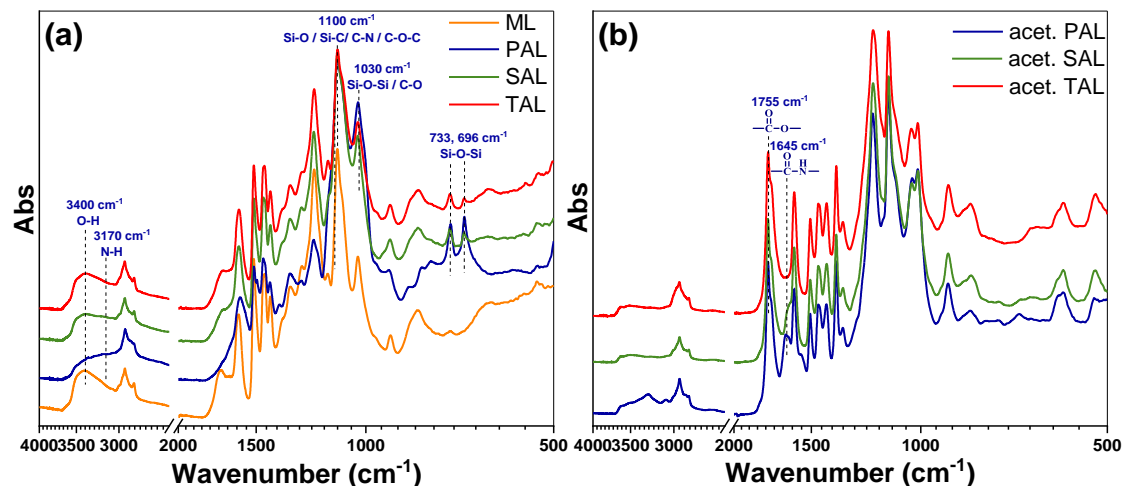


Fig. S1. (a) FTIR spectra of ML and ALs; (b) FTIR spectra of acetylated ML and acetylated ALs

Table S1. Elemental Contents and Surface Elemental Contents of ML, PAL, SAL, and TAL

Entry	Elemental Content				Particle Size (μm)
	C (%)	N (%)	O (%)	N/C (%)	
ML	63.07	0.73	29.64	1.30	8.7
PAL	60.81	2.40	30.04	3.93	12.5
SAL	61.14	1.98	30.02	3.25	12.0
TAL	61.46	1.60	29.94	2.60	9.3

S1 Adsorption Experiments

To evaluate effect of adsorbent dosage, heavy metal ion solutions with a concentration of 40 and 80 mg·L⁻¹ were prepared from Cd(NO₃)₂ and Pb(NO₃)₂, respectively. Next, 30 mL of the heavy metal ion solution was mixed with each AL (0.005–0.1 g) in an Erlenmeyer flask, and then adsorption experiments were performed without pH adjustment at a speed of 200 rpm, and 298.15 K for 1440 min. This result of adsorption experiment was listed in Fig. 1(a) and (b).

To investigate effect of pH, heavy metal ion solutions with a concentration of 40 and 80 mg·L⁻¹ were prepared from Cd(NO₃)₂ and Pb(NO₃)₂, respectively. The optimum dosage of PAL, SAL, and TAL for Cd(II) ions were 0.04 g, 0.06 g, and 0.1 g, respectively. Furthermore, the optimum dosage of PAL, SAL, and TAL for Pb(II) ions were 0.02 g, 0.06 g, and 0.06 g, respectively. Next, 30 mL of the heavy metal ion solution was mixed with each optimum dosage of ALs in an Erlenmeyer flask, and then adsorption experiments were performed with a pH of 3 to 7 at a speed of 200 rpm, and 298.15 K for 1440 min. This result of adsorption experiment was listed in Fig. 1(c) and (d).

To evaluate effect of setting time, heavy metal ion solutions with a concentration of 40 and 80 mg·L⁻¹ were prepared from Cd(NO₃)₂ and Pb(NO₃)₂, respectively. Next, 30 mL of the heavy metal ion solution was mixed with each optimum dosage of ALs in an Erlenmeyer flask, and then adsorption experiments were performed without pH adjustment at a speed of 200 rpm, and 298.15 K for 0 to 1440 min. This result of adsorption experiment was listed in Fig. 1(e) and (f).

To investigate adsorption isotherms, optimum dosage of ALs was added into 30 mL of Cd(II) ion solution (concentration gradient: 10-300 mg·L⁻¹) with a pH of 5.5 at 298.15 K for 1440 min. For Pb(II) ions adsorption, the optimum dosage of ALs, and the concentration of Pb(II) ion solution is 10-300 mg/L with a pH of 5.0 at 298.15 K for 1440 min. This result of adsorption experiment is listed in Fig. S3.

To investigate effect of temperature for metal ion adsorption, about optimum dosage of ALs was added into 30 mL of metal ion solution (concentration gradient: 40 mg·L⁻¹ for Cd(II) solution and 80 mg·L⁻¹ for Pb(II) solution) with a pH of 5.0 at 298.15, 313.15, and 333.15 K for 1440 min. This result is shown in Fig. S4.

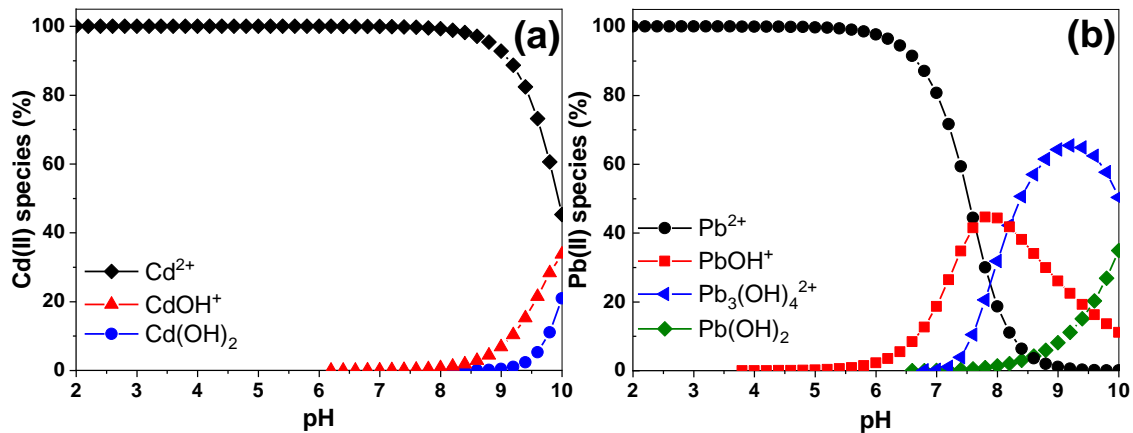


Fig. S2. Cadmium and lead species in the aqueous system as a function of pH by Visual MINTEQ (V3.0)

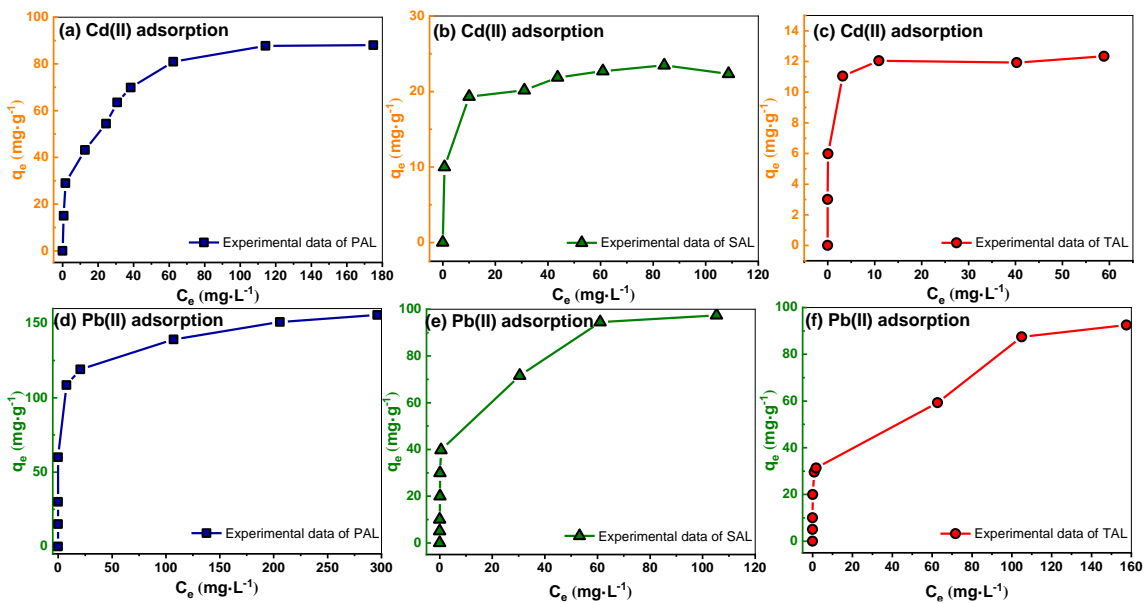


Fig. S3. Effect of initial concentration on Cd(II) ions adsorption capacity of PAL (a), SAL (b), and TAL (c) and Pb(II) ions adsorption capacity of PAL (d), SAL (e), and TAL (f)

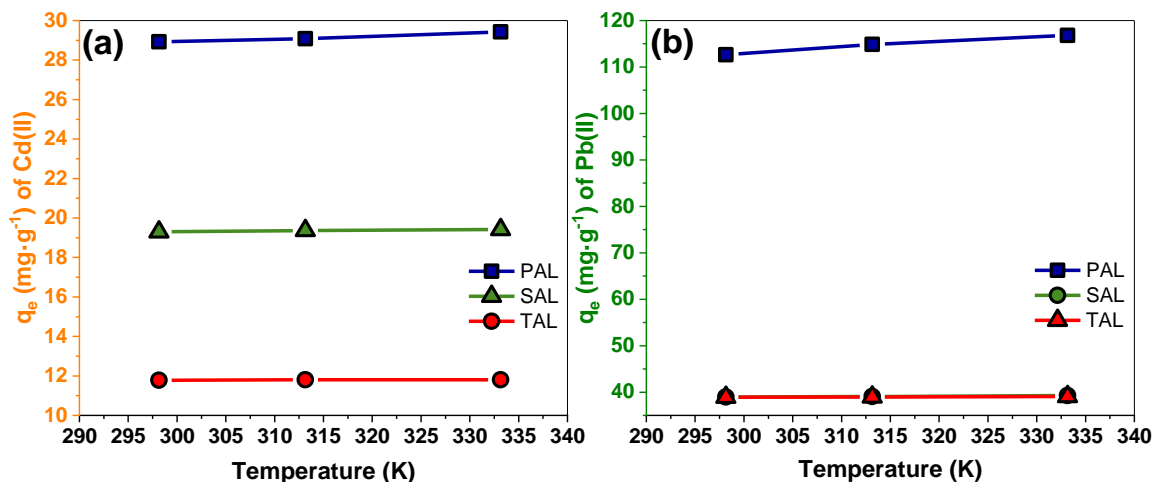


Fig. S4. (a) Cd(II) adsorption capacity of PAL, SAL, and TAL according to temperature (295.15, 313.15, and 333.15 K); (b) Pb(II) adsorption capacity of PAL, SAL, and TAL according to temperature (295.15, 313.15, and 333.15 K)

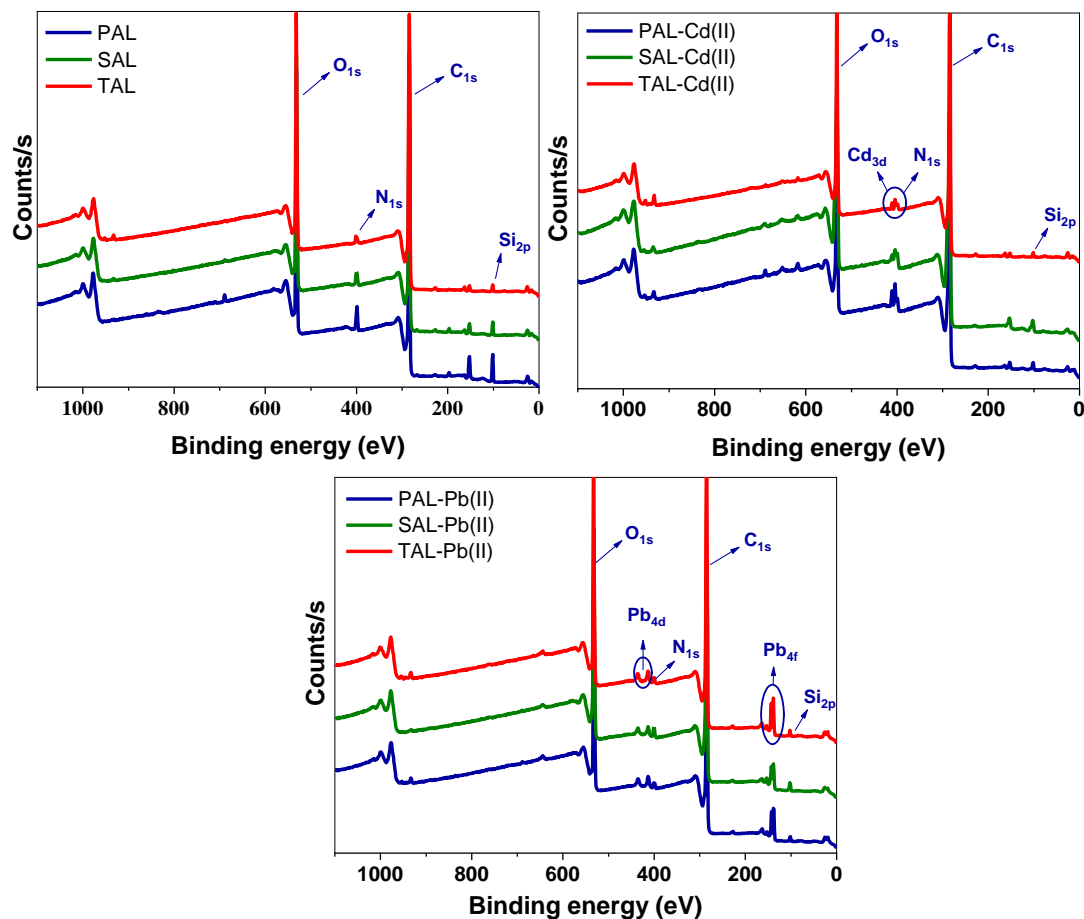


Fig. S5. (a) XPS survey spectra of ALs before adsorption; (b) XPS survey spectra of ALs after Cd(II) adsorption; (c) XPS survey spectra of ALs after Pb(II) adsorption

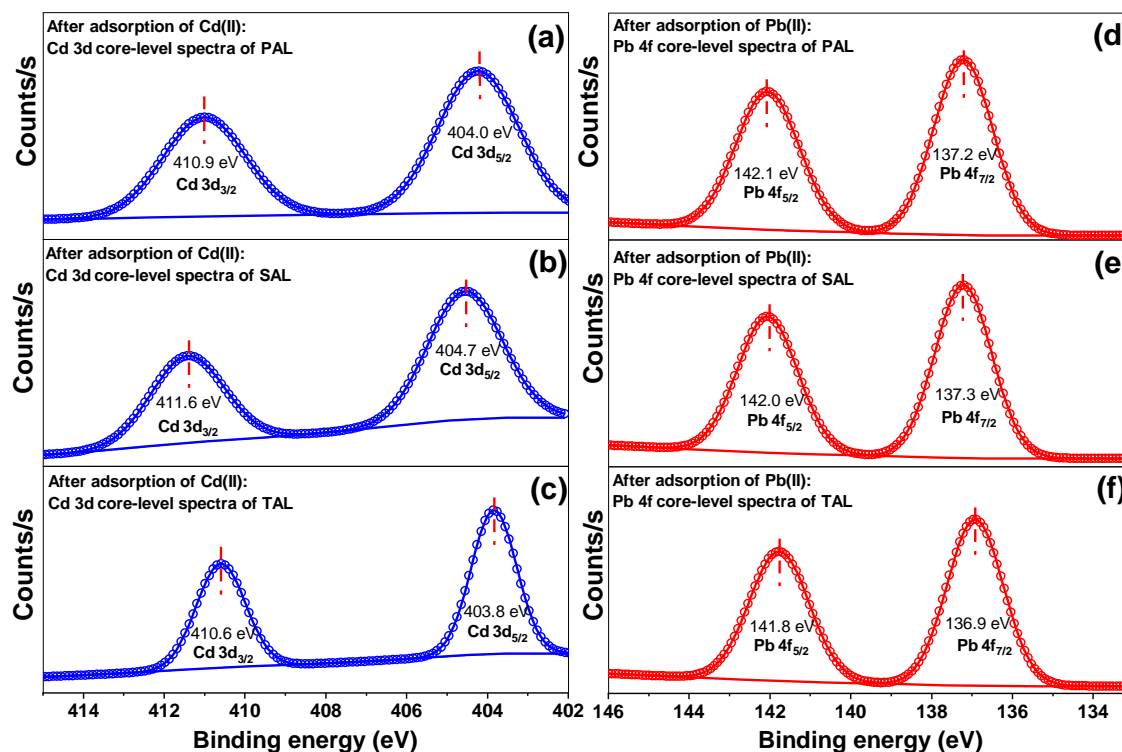


Fig. S6. Cd 3d spectrum after Cd(II) adsorption onto (a) PAL, (b) SAL, and (c) TAL; Pb 4f spectrum after Pb(II) adsorption onto (d) PAL, (e) SAL, and (f) TAL

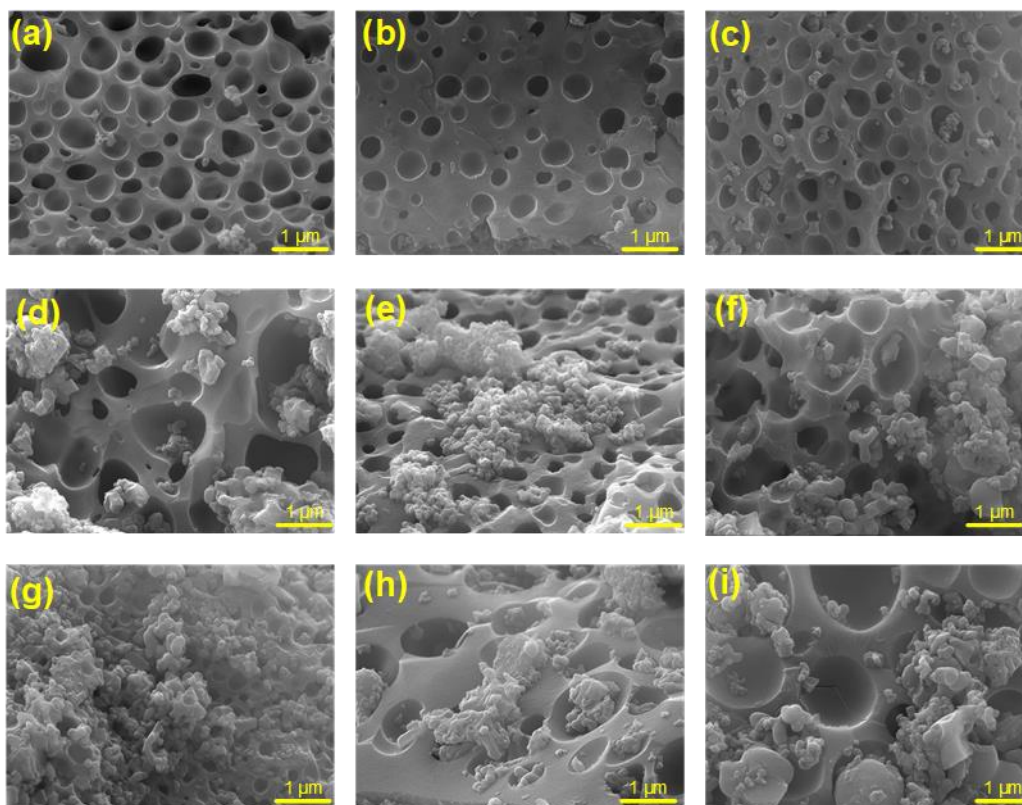


Fig. S7. Surface morphology of (a) PAL, (b) SAL, (c) and TAL before metal ion adsorption; surface morphology of (d) PAL, (e) SAL, and (f) TAL after Cd(II) adsorption; surface morphology of (g) PAL, (h) SAL, and (i) TAL after Pb(II) adsorption

Table S2. Surface element contents of ALs before and after Cd(II), and Pb(II) Adsorption from SEM-EDS

Element	Atomic %								
	PAL	PAL-Cd(II)	PAL-Pb(II)	SAL	SAL-Cd(II)	SAL-Pb(II)	TAL	TAL-Cd(II)	TAL-Pb(II)
C	83.1	72.8	68.4	79.9	69.8	72.6	78.1	73.9	74.7
N	1.5	4.2	1.1	1.5	4.5	1.0	0.9	4.1	0.7
O	14.8	17.3	15.7	17.7	22.1	18.2	18.4	18.5	18.7
Si	0.3	2.0	2.6	0.2	0.5	0.7	0.4	0.5	0.4
S	0.3	1.2	2.0	0.7	1.7	2.0	2.2	2.0	2.5
Cd	NA	2.5	NA	NA	1.5	NA	NA	1.1	NA
Pb	NA	NA	10.3	NA	NA	5.5	NA	NA	3.0

NA is not available.